Bulletin of the Seismological Society of America, Vol. 106, No. 4, pp. 1482–1498 August 2016, doi: 10.1785/0120150346

Estimation of the Coda-Wave Attenuation and Geometrical Spreading in the New Madrid Seismic Zone

by Farhad Sedaghati and Shahram Pezeshk

Abstract Using the single backscattering method, coda quality factor functions through coda window lengths of 20, 30, 40, 50, and 60 s have been estimated for the New Madrid seismic zone (NMSZ). Furthermore, geometrical spreading functions for distances less than 60 km have been determined in this region at different center frequencies exploiting the coda normalization method. A total of 284 triaxial seismograms with good signal-to-noise ratios (SNR > 5) from broadband stations located in the NMSZ were used. The database consisted of records from 57 local earthquakes with moment magnitudes of 2.6–4.1, and hypocentral distances less than 200 km.

Q-factor values were evaluated at five frequency bands with central frequencies of 1.5, 3, 6, 12, and 24 Hz. Vertical components were utilized to estimate vertical coda Q-factor values. Horizontal coda Q-factor values were determined using the average amount of the Q-factor values estimated from two orthogonal horizontal components. The coda Q-factor increases with increasing of the coda window length implying that with increasing the depth, the coda Q-factor increases. The intermediate values of the Q-factor and intermediate values of the frequency dependency indicate that the Earth's crust and upper mantle beneath the entire NMSZ is tectonically a moderate region with a moderate to relatively high degree of heterogeneities.

The geometrical spreading factors of S-wave amplitudes are frequency dependent and determined to be -0.761, -0.991, -1.271, -1.182, and -1.066 for center frequencies of 1.5, 3, 6, 12, and 24 Hz, respectively, at hypocentral distances of 10–60 km. The geometrical spreading factors for lower frequencies are not recommended to be used due to the greater impact of the radiation pattern and directivity effect on low frequencies, as well as the greater sensitivity of band-pass-filtered seismograms of small earthquakes to the noise in low frequencies.

Introduction

The attenuation of seismic waves is one of the main parameters in characterizing the medium through which the wave propagates. The amplitude of a seismic wave is dissipated with respect to the distance traveled from the source through the propagation path. This dissipation continues until the seismic wave disappears due to loss of energy. In addition to the reduction of the amplitude, attenuation distorts the phase part of a seismogram by delay, and this shift in the phase part causes velocity dispersion of seismic waves (Polatidis *et al.*, 2003; Montaña and Margrave, 2004; Ruan, 2012). The attenuation derives from the geometrical spreading, scattering, and intrinsic absorption (Kumar *et al.*, 2005; Padhy *et al.*, 2011; Shengelia *et al.*, 2011). A seismic wave initiates from a point source and it distributes over a spherical surface. The decay rate of the amplitude because of this spherical expansion of a wavefront is called the geometrical spreading. The elastic or scattering attenuation redistributes the wave energy. This attenuation is produced by heterogeneities in the Earth such as cracks and faults. In addition, refraction and reflection of waves and irregular topography cause the elastic attenuation (Sato and Fehler, 1998). The anelastic or intrinsic attenuation is described as the conversion of wave's energy into heat due to gradual absorption by the Earth. The reasons behind the anelastic attenuation are the friction and viscosity of the medium (Jackson and Anderson, 1974; Mitchell, 1995). It should be pointed out that the scattering attenuation only redistributes the energy of the seismic wave and the total energy in the wavefield remains constant, whereas the intrinsic attenuation causes disappearance of the seismic wave due to loss of energy. The effective quality factor is supposed to be a combination of the scattering attenuation and the intrinsic absorption (Dainty, 1981; Wennerberg, 1993; Polatidis *et al.*, 2003).

The combination of the quality factor and geometrical spreading functions describes the path effect. The path effect in the frequency domain can be defined as the multiplication of geometrical spreading and attenuation functions (Boore, 2003; Zandieh and Pezeshk, 2010)

$$P(R, f) = Z(R) \exp\left(-\frac{\pi f R}{Q(f) V_S}\right), \qquad (1)$$

in which $Z(R)$ is the geometrical spreading function, V_S is the average shear-wave velocity in the propagation path, f is the frequency, R is the hypocentral distance, and $Q(f)$ is a dimensionless parameter describing the quality factor function. The attenuation is proportional to the inverse of the quality factor Q^{-1} and is defined as (Knopoff and Hudson, 1964; Jackson and Anderson, 1974)

$$Q^{-1} = \frac{1}{2\pi}\frac{\Delta E}{E}, \qquad (2)$$

in which ΔE is the energy lost per cycle and E is the total energy. Path effect can be used to understand the source mechanism (Abercrombie and Leary, 1993; Abercrombie, 1995; Zeng and Anderson, 1996) and site response (Bonilla *et al.*, 1997) to simulate time histories and to develop ground-motion prediction equations (GMPEs) or ground-motion models (GMMs) for the seismic-hazard assessment, especially for areas with sparse earthquake records and tectonic interpretation.

Data analysis associated with events occurring in central and eastern North America (CENA) and southeastern Canada demonstrates that the decay of the Fourier amplitudes of seismic waves with respect to the distance may be a combination of three different segments. This hinged-trilinear geometrical spreading function has a steep decay for distances within approximately 70 km and less steep decay for distances beyond around 140 km. Between 70 and 140 km, there is almost no attenuation, and in several studies the amplitude increases with increasing the distance. This transition zone results from large amplitude postcritical reflections from Moho discontinuity (Burger *et al.*, 1987; Atkinson and Mereu, 1992). Pezeshk *et al.* (2015) used hinge points at 60 and 120 km instead of 70 and 140 km to be consistent with the path duration proposed by Boore and Thompson (2015).

Atkinson and Mereu (1992) reported a geometrical spreading of $R^{-1.1}$ for distances within 70 km and R^0 for distances between 70 and 130 km, using 1200 vertical-component seismograms out of 100 small-to-moderate magnitude earthquakes in southeastern Canada. They used the shear-wave phases that include the direct arrival to derive geometrical spreading factors for distances up to 130 km. Samiezade-Yazd *et al.* (1997) evaluated nearly 2200 vertical traces from 237 earthquakes recorded at 83 stations located in the New Madrid seismic zone (NMSZ) and proposed a geometrical spreading of $R^{-1.0}$ for distances less than 50 km, and $R^{-0.25}$ for distances between 50 and 120 km. The authors utilized the coda normalization method to find geometrical spreading functions for the direct S wave. Atkinson (2004) investigated the decay of Fourier spectral amplitudes of 1700 seismograms out of 186 small-to-moderate earthquakes in southeastern Canada and the northeastern United States, and determined a geometrical spreading of $R^{-1.3}$ for distances less than 70 km and $R^{+0.2}$ for distances between 70 and 140 km. Atkinson (2004) used the shear-wave phases to estimate geometrical spreading functions. Zandieh and Pezeshk (2010) obtained a geometrical spreading of $R^{-1.0}$ for distances out to 70 km and $R^{+0.25}$ for distances between 70 and 140 km, using 500 vertical-component seismograms from 63 small-to-moderate magnitude earthquakes in the NMSZ. They compared the whole waveform length and shear window and found that Fourier amplitudes derived from both cases for records used in this study are very similar. Chapman and Godbee (2012) reported geometrical spreading functions of $R^{-1.3}$ and $R^{-1.5}$ for strike-slip and reverse fault mechanisms, respectively, for the geometric mean of horizontal components for rock sites at distances less than 60 km based on records from eastern North America (ENA). In their study, the shear-wave window is used. Atkinson and Boore (2014) investigated the decay of the Fourier amplitudes of the shear wave for earthquakes that occurred in ENA and were recorded on rock sites and estimated a geometrical spreading of $R^{-1.3}$ for distances less than 50 km and $R^{-0.5}$ for distances beyond 50 km. Frankel (2015) evaluated the attenuation of the Fourier amplitudes of S waves for seven small-to-moderate magnitude earthquakes in Charlevoix, Quebec, Canada, and determined geometrical spreading functions of $R^{-1.52}$, $R^{-1.21}$, and $R^{-0.79}$ for distances less than 80 km at central frequencies of 1, 5, and 14 Hz, respectively. The author utilized the coda normalization method to find geometrical spreading functions at different frequencies for the direct S wave.

According to a point source with an isotropic radiation pattern in a homogenous elastic whole space, the geometrical spreading $Z(R)$ is expected to be proportional to the inverse of the hypocentral distance $R^{-\alpha}$ and the exponent α is expected to be frequency independent. However, the geometrical spreading is more sophisticated than a frequency-independent function of the distance, because in reality, the source is a finite fault, the radiation pattern is anisotropic, and the Earth's structure is heterogeneous (Chapman and Godbee, 2012; Frankel, 2015).

The amount of Q aids in distinguishing the seismicity and tectonic activity of the region under study because seismic waves are attenuated faster in seismically active areas. Therefore, once the quality factor is a large number, it reveals that seismic waves are damped at a slower pace, and accordingly, the region is tectonically stable. In general, an area with $Q < 200$ may be classified as an active area, and an area with $Q > 600$ may be considered as a stable area (Mitchell, 1995; Sato and Fehler, 1998; Kumar *et al.*, 2005; Sertçelik, 2012). Moreover, if the ratio of $Q_P^{-1}/Q_S^{-1} > 1$ for the frequency greater than 1 Hz in which Q_P^{-1} is the attenuation of P waves and Q_S^{-1} is the attenuation of S waves, it implies that the region may be seismically active (Sato, 1984).

The quality factor can be estimated using frequency-domain techniques (Anderson and Hough, 1984; Chen *et al.*, 1994; Zandieh and Pezeshk, 2010; Mousavi *et al.*, 2014; Hosseini *et al.*, 2015), or time-domain techniques (Wu and Lees, 1996; Zollo and de Lorenzo, 2001) for different phases of seismic waves such as body waves (primary and shear waves), surface waves, and coda waves regarding the frequency band of interest. For high frequencies, laboratory techniques are suggested, while for low frequencies, deterministic techniques are often applied. For moderate frequency range, which is the band of interest for seismologists and structural engineers, statistical approaches are preferred rather than deterministic approaches (Pulli, 1984).

The quality factor is frequency dependent and is defined by a power-law equation at a specific frequency as (Singh and Herrmann, 1983)

$$Q(f) = Q_0 f^{\eta}, \tag{3}$$

in which Q_0 is the quality factor at 1 Hz, f is the frequency, and η is a constant.

Several researchers (Al-Shukri *et al.*, 1988; Chen *et al.*, 1994; Liu *et al.*, 1994; Samiezade-Yazd *et al.*, 1997; Jemberie and Langston, 2005; Zandieh and Pezeshk, 2010) investigated the attenuation of the NMSZ using various methods. One of the goals of this article is to determine the quality factor for coda waves in the NMSZ using a time-domain technique based on the amplitudes of coda waves. Another goal of this article is to investigate the geometrical spreading utilizing the coda normalization technique. In this regard, first a database containing 284 three-component waveform seismograms is selected. Then, Q_C values for coda waves are computed using the single backscattering method (Aki, 1969; Aki and Chouet, 1975). This method is based upon the decay rate of coda-wave amplitudes on narrow-frequency band-pass-filtered seismograms. Finally, this method is implemented using the selected database and results are compared to results obtained from previous studies for the NMSZ as well as results reported for other tectonically stable and active regions. One new aspect of this study compared to other coda quality factor studies is that vertical and horizontal coda quality factor functions are estimated, and a comparison between them is performed to determine whether or not there are any discrepancies between vertical and horizontal coda quality factor functions. In this study, the vertical coda quality factor refers to the quality factor derived from the coda of vertical components, and the horizontal coda quality factor refers to the quality factor computed from the coda of horizontal components. In addition, the decay rates of the amplitudes of *S* waves with the hypocentral distance are estimated by normalizing the *S* waves amplitudes with respect to the coda waves amplitudes at a fixed time from the origin time to remove the source spectrum and the site response (Aki, 1980a; Yoshimoto *et al.*, 1993; Frankel, 2015). To this end, horizontal components of 160 out of 284 seismograms, which have hypocentral distances less than 60 km, are considered to evaluate the geometrical spreading functions for the NMSZ.

Tectonic Setting

According to Nuttli and Zollweg (1974) and Baqer and Mitchell (1998), the eastern side of the Rocky Mountains to the Atlantic coast containing CENA has various seismic and tectonic characteristics such as seismic-wave attenuation, as compared to the western side of the Rocky Mountains to the Pacific coast. For instance, an area over five million square kilometers was shaken due to the main earthquake of the historic series of 1811–1812 in the NMSZ; on the other hand, the San Francisco earthquake of 1906 was felt in an area of only about one million square kilometers despite having quite the same magnitude (Nuttli, 1973a,b; Elnashai *et al.*, 2009). According to reliable available reports, the 1811–1812 sequences were felt in places located up to 1700 km away from the epicenters (Ramírez-Guzmán *et al.*, 2015), while for the 1906 earthquake, the maximum epicentral distance extended only up to approximately 900 km (Aagaard *et al.*, 2008). This indicates that earthquakes in the CENA can affect much larger areas in comparison to earthquakes with similar magnitudes in the western United States.

Following Dreiling *et al.* (2014), CENA is classified into four different regions (Fig. 1) due to their discrepant geologies and tectonic settings: the Atlantic coastal plain, the Appalachian province, central North America (CNA), and the Mississippi embayment/Gulf Coast region (MEM). The NMSZ is located in the MEM region, near the southern border of CNA, which has dissimilar and unique attenuation properties compared to the other three regions of CENA (Dreiling *et al.*, 2014). The NMSZ is considered to be a region with an intraplate (within a tectonic plate) seismicity that is surrounded by a roughly stable crust (Al-Shukri *et al.*, 1988) and is undergoing compressional stress (Liu and Zoback, 1997). This region comprises several faults within the Cambrian Reelfoot rift that stretches from Cairo, Illinois, to Marked Tree, Arkansas, with an approximate length of 200 km (Tavakoli *et al.*, 2010; Talwani, 2014). The Cambrian Reelfoot rift, which was reactivated by tensional or compressional stresses corresponding to plate tectonic interactions during Mesozoic, has formed during the late Precambrian to the early Cambrian due to the continental breakup (Braile *et al.*, 1986). The majority of faults responsible for earthquakes occurring in the NMSZ are deeply embedded beneath the relatively thick layers of sediments; hence, understanding the nature and behavior of the faults is very sophisticated.

The historic earthquake sequence of 1811–1812 as well as frequent smaller earthquakes indicate the potential of generating a large and damaging earthquake (Al-Shukri *et al.*, 1988; Liu *et al.*, 1994). Therefore, due to this potential in the NMSZ, this region is of great interest to seismologists and earthquake engineers to further prepare for a high-magnitude earthquake.

Methodology

Coda Quality Factor Estimation

Based on the distance between the source and station, earthquakes can be classified into three different groups: local, regional, and teleseismic earthquakes. Local events are defined as earthquakes with distances less than about

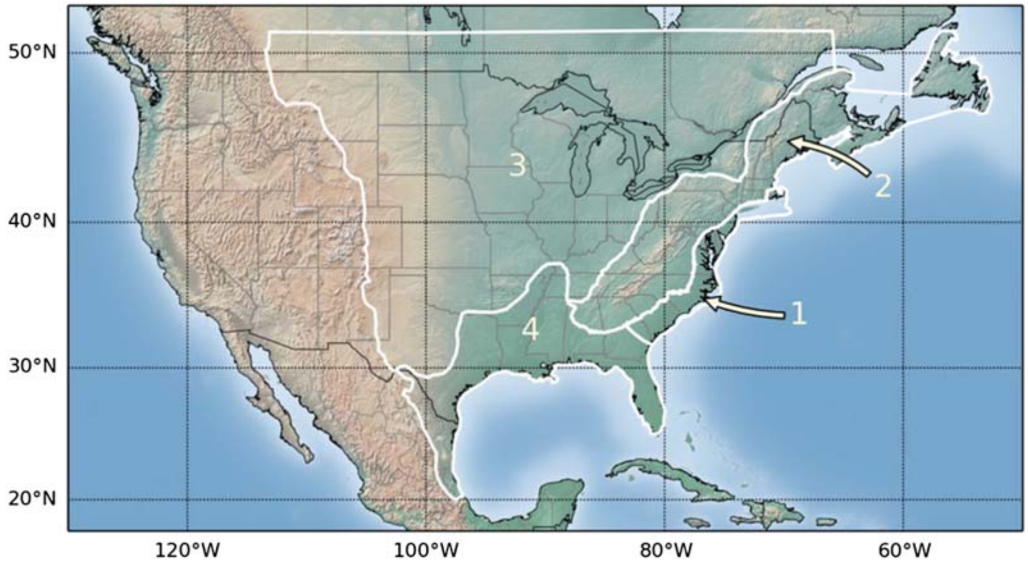

Figure 1. Pacific Earthquake Engineering Research (PEER) Next Generation Attenuation-East (NGA-East) ground-motion regionalization (from Dreiling *et al.*, 2014). Regions 1, 2, 3, and 4 are Atlantic coastal plain, Appalachian province, central North America (CNA), and Mississippi embayment/Gulf Coast region (MEM), respectively. The color version of this figure is available only in the electronic edition.

200–500 km. Coda is considered as the tail of a local seismogram and includes short-period waves (high frequency up to 25 Hz). The coda wave is interpreted as a superposition of backscattering body waves from heterogeneities distributed randomly but uniformly in the Earth's crust and upper mantle (Aki, 1969; Aki and Chouet, 1975). Coda waves may be utilized to compute the local earthquake magnitude, the seismic moment, and the coda quality factor (Aki, 1969; Aki and Chouet, 1975; Herrmann, 1975; Bakun and Lindh, 1977).

The quality factor for coda waves Q_C can be acquired through two different techniques: the scattering method and the energy-flux method. The single backscattering model was first proposed by Aki (1969) and then developed by Aki and Chouet (1975) to estimate Q_C. According to Aki and Chouet (1975), even though the coda envelope decay rate is independent of the distance between the source and receiver and magnitude, it depends on the lapse time from the origin time of the event. In addition, they assumed that scattering is a weak process and is not strong enough to generate secondary waves once they encounter other scatters. This approximation is called the Born approximation. Scattered waves are produced once seismic waves encounter heterogeneities, faults, cracks, or irregular topography (Kumar *et al.*, 2005). Later, Sato (1977) developed the single backscattering method and incorporated the source-receiver offset using the single isotropic scattering approximation. Rautian and Khalturin (1978) pointed out that if the inception of the coda is less than twice of the shear-wave onset, the source-receiver offset should be taken into account; otherwise, the effect of the source-receiver distance is not significant. Kopnichev (1977) figured out that the earlier part of the coda wave is dominated by single scattered waves, whereas for the later part of the coda the effect of secondary and tertiary scattered waves is not negligible. Then, Gao *et al.* (1983) expanded the single scattering method to the multiple scattering method and considered the secondary and tertiary backscattered body waves. They concluded that if the lapse time for the coda is less than 100 s, the effect of secondary and tertiary backscattered waves can be neglected; however, for longer lapse-time, relationships should account for those waves. In the second technique, the energy-flux method, proposed by Frankel and Wennerberg (1987), they presumed that after a lapse time from the source excitation, the coda energy would be uniformly distributed in the Earth's crust and upper mantle.

In the single backscattering model, the coda amplitude for an assumed frequency band A_C at the central frequency of the assumed frequency band f and a specific lapse time from the earthquake origin time t can be written as

$$A_C(f,t) = S(f)\left[t^{-\alpha_C}\exp\left(-\frac{\pi f t}{Q_C(f)}\right)\right]G(f)I(f), \quad (4)$$

in which $S(f)$, $G(f)$, $I(f)$, and $Q_C(f)$ denote the source response, the site amplification, the instrument response, and the coda-wave quality factor, respectively. These amounts are constant for a specific frequency. The parameter α_C represents the geometrical spreading coefficient and is set to 1, 0.5, and 0.75 for body waves, surface waves, and diffusive waves, respectively (Sato and Fehler, 1998). By substituting $\alpha_C = 1$, because coda waves are backscattered body waves (Aki, 1969, 1980a), and by taking a natural logarithm from both sides of equation (4), we get

$$\ln[A_C(f,t)\times t] = \ln[S(f)G(f)I(f)] - \frac{\pi f}{Q_C(f)}t = C - Bt. \quad (5)$$

Because $S(f)$, $G(f)$, and $I(f)$ are time independent, the natural logarithm of the multiplication of them is also time independent. In this regard, this equation is a simple linear equation and the slope B and the intercept C can be determined using the least-squares method. Consequently, Q_C is given by

$$Q_C(f) = \frac{\pi f}{B} \,. \tag{6}$$

It should be mentioned that Q_C represents a combination of intrinsic and scattering quality factors (Gao *et al.*, 1983; Jin and Aki, 1988; Polatidis *et al.*, 2003; Giampiccolo *et al.*, 2004). Wennerberg (1993) developed a method in which Q_C values derived from the single backscattering method (Aki and Chouet, 1975) can be separated into values of intrinsic and scattering quality factors using the multiple scattering approximation proposed by Zeng (1991).

The single isotropic model developed by Sato (1977) is expressed as

$$A_C(f,t,r) = S(f)\left[r^{-\alpha_C}\sqrt{\kappa(a)}\exp\left(-\frac{\pi f t}{Q_C(f)}\right)\right]G(f)I(f)\,, \tag{7}$$

in which α_C is considered to be 1 for body waves and r is the hypocentral distance; and $\kappa(a)$ is given by

$$\kappa(a) = \frac{1}{a}\ln\left(\frac{a+1}{a-1}\right), \tag{8}$$

in which a is

$$a = \frac{t}{t_S}\,, \tag{9}$$

in which t_S is the arrival time for the direct shear wave. $\kappa(a)$ increases the amplitude of the coda wave at lapse times close to the shear-wave arrival. This approach is useful once the background noise level is high and the coda amplitude would be lost in the noise at larger lapse times; and consequently, it is needed to use shorter lapse times. Moreover, when the length of signals are short, the shorter lapse times must be used; and accordingly, the single backscattering method cannot be utilized.

Pulli (1984) and Scherbaum and Kisslinger (1985) pointed out that Q_C is the average of the quality factor for an ellipsoidal volume with the source and receiver as its focus. Hence, the area inside which the coda waves are generated is an elliptical surface with the following equation:

$$\frac{x^2}{(V_S t_{\mathrm{avg}}/2)^2} + \frac{y^2}{(V_S t_{\mathrm{avg}}/2)^2 - (\Delta/2)^2} = 1\,, \tag{10}$$

in which V_S is the average shear-wave velocity in the propagation path, Δ is the average of hypocentral distances, and x and y represent the surface coordinates. The average lapse time (Havskov *et al.*, 1989) is also defined as

$$t_{\mathrm{avg}} = t_{\mathrm{start}} + \frac{W}{2}\,, \tag{11}$$

in which t_{start} is the initiation time of the coda window and W is the coda window length. Plus, the average depth of the assumed ellipsoid representing the penetration depth of the estimated coda quality factor (Havskov *et al.*, 1989) can be calculated by

$$h = h_{\mathrm{avg}} + \sqrt{\left(\frac{V_S t_{\mathrm{avg}}}{2}\right)^2 - \left(\frac{\Delta}{2}\right)^2}\,, \tag{12}$$

in which h_{avg} is the average of focal depths.

Geometrical Spreading

The single station coda normalization method proposed by Aki (1980a) is a time-domain technique to calculate the attenuation of the S wave for waveforms recorded at a specific station. Later, Frankel *et al.* (1990) showed that because the coda energy is uniformly distributed in the Earth's crust and upper mantle, coda amplitude decay rates are similar among different stations. Hence, the single station coda normalization method can be applied to earthquakes recorded on multiple stations. According to Aki (1980a), the amplitude of the S wave of a seismogram $A_S(f,R)$ at a specific frequency f and for a particular hypocentral distance R can be written as

$$A_S(f,R) = CS(f)\left[R^{-\alpha_S}\exp\left(-\frac{\pi f R}{Q_S(f)V_S}\right)\right]G(f)I(f)\,, \tag{13}$$

in which C is the source radiation pattern factor for the S wave, $R^{-\alpha_S}$ denotes the geometrical spreading function, V_S is the average shear-wave velocity in the propagation path, Q_S represents the S-wave quality factor, and the remaining terms have been previously defined. In the coda normalization technique, the effects of the source and site are removed by dividing the amplitude of the S wave into the amplitude of the coda wave at a specific time elapsed from the origin time. Because the amplitude of the coda wave is independent of the distance, equation (4) can be rewritten as

$$A_C(f,t_C) = S(f)P(f,t_C)G(f)I(f)\,, \tag{14}$$

in which t_C is a specific lapse time from the origin time of the event and $P(f,t_C)$ denotes the path effect that is dependent on t_C. It should be pointed out that the coda amplitude is not dependent on the radiation pattern (Aki, 1969). Dividing equation (13) by equation (14), the following equation is obtained:

$$\frac{A_S(f,R)}{A_C(f,t_C)} = \frac{C}{P(f,t_C)}\left[R^{-\alpha_S}\exp\left(-\frac{\pi f R}{Q_S(f)V_S}\right)\right], \tag{15}$$

and then, by moving the exponential term to the other side and taking a natural logarithm from both sides of the above-mentioned equation, it can be written as

$$\ln\left[\frac{A_S(f,R)}{A_C(f,t_C)} \times \exp\left(\frac{\pi f R}{Q_S(f)V_S}\right)\right] = -\alpha_S \ln(R) + \ln\left[\frac{C}{P(f,t_C)}\right]. \tag{16}$$

Table 1
Center for Earthquake Research and Information (CERI) Stations

Station	Location	Longitude (°)	Latitude (°)	Number of Records	Sensor Type	Sampling Frequency (Hz)
GLAT	Glass, Tennessee	−89.288	36.269	36	CMG40T	100
GNAR	Gosnell, Arkansas	−90.018	35.965	29	CMG40T	100
HALT	Halls, Tennessee	−89.340	35.911	27	CMG40T	100
HBAR	Harrisburg, Arkansas	−90.657	35.555	10	CMG40T	100
HENM	Hickman, Kentucky	−89.472	36.716	26	CMG40T	100
HICK	Henderson Mound, Missouri	−89.229	36.541	35	CMG40T	100
LNXT	Lenox, Tennessee	−89.491	36.101	27	CMG40T	100
LPAR	Lepanto, Arkansas	−90.300	35.602	16	CMG40T	100
PARM	Stahl Farm, Missouri	−89.752	36.664	34	CMG40T	100
PEBM	Pemiscot Bayou, Missouri	−89.862	36.113	17	CMG40T	100
PENM	Penman Portageville, Missouri	−89.628	36.450	27	CMG40T	100

The slope of the above-mentioned equation can be simply acquired using the least-squares method, because the $\ln[\frac{C}{P(f,t_C)}]$ term is distance independent. Therefore, the geometrical spreading factor for S waves, α_S, can be obtained from the gradient of the fitted line for this equation.

Database

The initial database containing 500 three-component digital waveforms from 63 local events that occurred during the period of 2000–2009 in the NMSZ and recorded by the Center for Earthquake Research and Information (CERI) at the University of Memphis are used for the present study (see Data and Resources). This database is the same as the one employed by Zandieh and Pezeshk (2010) and Zandieh and Pezeshk (2011) to investigate the path effect of vertical-component ground motions and horizontal-to-vertical-component spectral ratios in the NMSZ, respectively.

All CERI stations are equipped with broadband Güralp CMG-40T triaxial seismometers, which have a flat velocity response for the frequency range of 0.033–50 Hz and sampling frequency of 100 Hz. The details of these stations are provided in Table 1.

Every single record has been visually inspected and the ones with poor quality or poor signal-to-noise ratio (SNR < 5) are discarded from the database. SNR for each record is defined as the ratio of the root mean square (rms) amplitude of a 5-s window after onset of the P wave over the rms amplitude of a 5-s window before the P-wave arrival. Furthermore, the maximum hypocentral distance is restricted to 200 km, and records with hypocentral distances greater than 200 km are removed, because for large hypocentral distances, the coda-wave amplitude is dependent on the hypocentral distance (Yoshimoto *et al.*, 1993). Finally, the selected database consists of 284 three-component seismograms from 57 local earthquakes with moment magnitude **M** between 2.6 and 4.1. Focal depths for these events are less than 25 km and the majority of them have focal depths around 10 km. Figure 2 depicts a map of the CERI seismic network as well as the location of the considered events. It should be noted that the size of the star signs has been scaled based on the magnitude in Figure 2. Figure 3 illustrates the distribution of the data with respect to the hypocentral distance versus magnitude. We should mention that all earthquakes used in this study are local events with hypocentral distances less than 200 km and focal depths down to 25 km.

Data Processing

All three components of velocity waveforms are utilized for the estimation of Q_C. Vertical components of seismograms are used to estimate the vertical coda quality factor Q_C^V. To compute the horizontal coda quality factor Q_C^H, first Q_C is individually determined for each horizontal component. Then, the average amount at each frequency band is considered as the horizontal coda quality factor for that frequency band. The origin time of each seismogram is calculated through the P- and S-wave arrival times assuming $V_P/V_S = 1.73$ (Dreiling *et al.*, 2014). Then, the baseline correction is performed on every single seismogram through subtracting the mean from the raw waveform and removing the linear trend to avoid confronting any biases.

Next, employing a phaseless eight-pole Butterworth filter for five passbands with a bandwidth of $0.667f$ in which f is the central frequency (see Table 2), all velocity waveforms are digitally band-pass filtered. It should be noted that using the usual Butterworth filter introduces a phase delay, and accordingly, causes distortion in the signal. Therefore, a zero-phase (phaseless) Butterworth filter is used to avoid changing the size and position of the peaks in waveforms. Band-pass-filtered seismograms for the 20 June 2005 earthquake (36.93° N, 88.99° W; **M** 2.7; and 9.8 km depth), which were recorded at the station LNXT with an epicentral distance of 102 km at central frequencies of 1.5, 3, 6, 12, and 24 Hz, are demonstrated in Figure 4. According to Mukhopadhyay and Sharma (2010), the quality factor slightly increases once the start time of the coda window increases. In this study, we use a coda window beginning from twice the shear-wave arrival to avoid contamination of the direct S wave in the coda wave (Rautian and Khalturin, 1978).

The amplitude of the coda wave given by the following equation (Woodgold, 1994; Rahimi and Hamzehloo, 2008) is

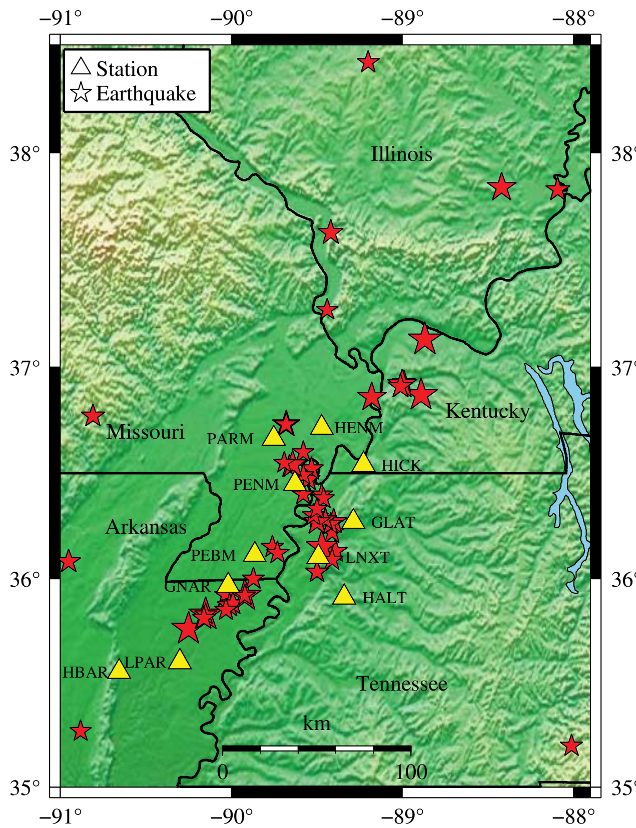

Figure 2. Locations of the considered events and Center for Earthquake Research and Information (CERI) broadband stations. The color version of this figure is available only in the electronic edition.

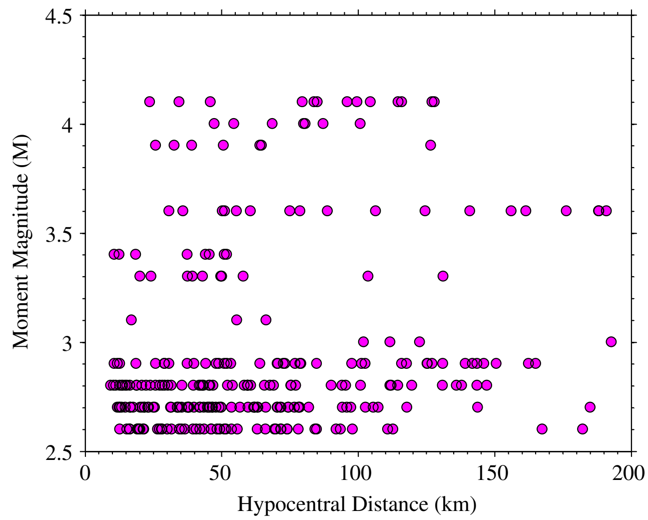

Figure 3. Distribution of the database with respect to the hypocentral distance versus magnitude. The color version of this figure is available only in the electronic edition.

estimated using the envelope function of the coda amplitude by applying the Hilbert transform

$$A(f,t) = \sqrt{[x(f,t)]^2 + [H(x(f,t))]^2}, \qquad (17)$$

in which x is the amplitude of the band-pass-filtered seismogram at the central frequency f and a lapse time measured from the earthquake origin time t. H represents the Hilbert transform.

The rms value of the amplitudes is evaluated for a moving window with a length of 5 s centered at lapse time t to generate a smoother coda envelope. Then, the moving window slides along the coda window with steps of 1 s. Using rms values instead of using direct Fourier transform leads to obtaining more stable results (Frankel, 2015). We do not use all rms values obtained from the moving window and discard centers in which the rms value to noise ratio is less than 2. As defined earlier, the noise amplitude is the rms value in a window of 5 s length before the P-wave arrival. This process aims to acquire coda quality factor values with better correlation coefficients.

Diverse coda window lengths are defined to investigate the effect of the depth on the quality factor (Pulli, 1984; Del Pezzo *et al.*, 1990; Woodgold, 1994). Havskov and Ottemöller (2005) suggested a minimum value of 20 s for the coda window length to obtain stable results. Of course, there are a few studies that obtained stable results for coda window lengths of 15 or 10 s (Del Pezzo *et al.*, 1990; Padhy *et al.*, 2011). In this study, coda window length varies from 20 to 60 with increments of 10 s. Although there is generally no limit on the maximum length of the coda window, the values of SNR > 2 condition for most of the seismograms in this study cannot be satisfied for coda window lengths more than 60 s. Thus, the maximum length of the coda window is restricted to 60 s.

All assumed lapse times are less than 100 s and the inception times of the coda waves are supposed to be greater than twice the beginning of direct shear waves. Therefore, the single backscattering model with no distance between the source and receiver has been selected to estimate the quality factor for coda waves. Finally, having values of the smoothed coda amplitude for the centers of sliding windows, Q_C can be obtained from the gradient of the fitted line (equation 4) using the least-squares method at each frequency band (Fig. 5). It should be pointed out that during the estimation of Q_C values, some negative numbers are obtained. Following Woodgold (1994), these negative amounts are deleted before averaging Q_C values at each frequency band.

To evaluate the geometrical spreading function, the rms values of the envelopes of the band-pass-filtered seismo-

Table 2
Frequency Bands

Band	Low Cutoff Frequency (Hz)	Central Frequency (Hz)	High Cutoff Frequency (Hz)
1	1	1.5	2
2	2	3	4
3	4	6	8
4	8	12	16
5	16	24	32

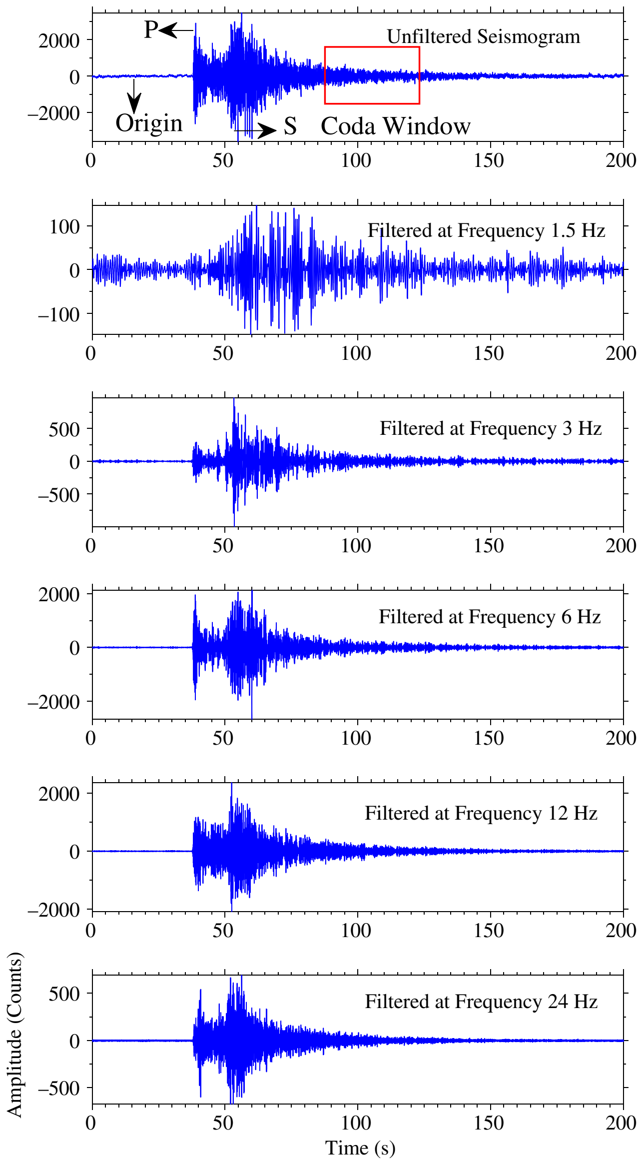

Figure 4. Band-pass-filtered seismograms (vertical component) for the 20 June 2005 earthquake (36.93° N; 88.99° W; **M** 2.7; and 9.8 km depth) recorded at the station LNXT with an epicentral distance of 102 km at central frequencies of 1.5, 3, 6, 12, and 24 Hz. Origin, *P*, and *S* represent origin time, *P*-wave arrival, and *S*-wave arrival. The color version of this figure is available only in the electronic edition.

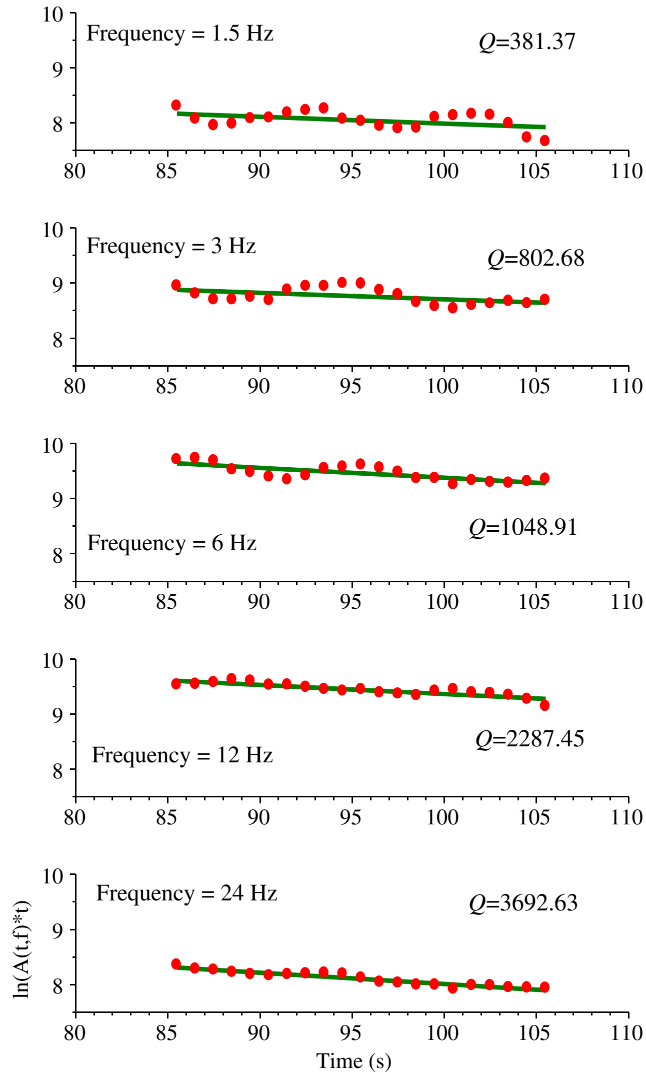

Figure 5. Estimation of the vertical Q_C values at each frequency band for the 20 June 2005 earthquake (36.93° N; 88.99° W; **M** 2.7; and 9.8 km depth) recorded at the station LNXT with an epicentral distance of 102 km with a coda window length of 20 s. The color version of this figure is available only in the electronic edition.

grams in time windows with various lengths are used to measure the amplitudes *S* waves and coda waves (Yoshimoto *et al.*, 1998; Padhy *et al.*, 2011; Tripathi *et al.*, 2014; Frankel, 2015). Equation (17) is used to acquire the envelope of each band-pass-filtered seismogram. To determine *S*-wave amplitudes, corresponding time windows begin from the *S*-wave arrival with a length of 5 s over horizontal components of band-pass-filtered seismograms. For the estimation of coda-wave amplitudes, various time windows are considered to assess the effect of the length and location of time windows on the derived geometrical spreading factor. Five time windows with a length of 5 s centered at 60, 70, 80, 90, and 97.5 s as well as a time window with a length of 40 s centered at 80 s are used in this study. These t_C are selected because they are greater than twice the *S*-wave arrival time of all the selected records and they are also less than 100 s to neglect the effects of secondary and tertiary backscattered waves. It should be pointed out that the ratio of the *S* wave to coda wave is obtained from the geometric mean of the ratios of the two horizontal components. The *S*-wave velocity of 3.58 km/s is used in this study (Dreiling *et al.*, 2014).

Results and Discussion

For each station, vertical and horizontal coda *Q*-factor values have been computed for five frequency bands. Then, the frequency-dependent equations of the coda quality factor values have been obtained from the power-law equation

(equation 2). Results are presented in Tables 3 and 4 for different coda window lengths (20, 30, 40, 50, and 60 s). The average amounts of Q_C^V and Q_C^H for the whole area under study are also reported in Tables 3 and 4. Figure 6 displays mean values as well as fitted lines of Q_C^V and Q_C^H for the whole region as a function of the frequency for assumed lengths of the coda window. We found that average quality factor values at each frequency estimated from all window lengths are very similar to quality factor values estimated from a window length of 40 s. Based on Tables 3 and 4, and according to Figure 6, the frequency-dependent nature of the Q-factor can be observed. The intermediate values of η manifest that the Earth's crust and upper mantle in the NMSZ may be considered as a relatively heterogeneous medium (Del Pezzo, 2008). This result is in good agreement with the result from Langston (2003). Langston (2003), using body-wave phases, inferred that the Mississippi embayment has a high level of lateral heterogeneities. In addition, because the estimated coda quality factor amounts range from 350 to 690, the area may be categorized as a region between tectonically active and stable regions (Mitchell, 1995; Sato and Fehler, 1998; Kumar *et al.*, 2005; Sertçelik, 2012). Furthermore, Figure 6 illustrates that with increasing coda window length, the coda quality factor increases, which means that the propagation path becomes more homogenous with increasing depth. It is worth noting that this effect is more sensitive to low frequencies than to high frequencies. Aki (1980a,b) and Roecker *et al.* (1982) stated that Q values tend to converge at high frequencies (around 20 Hz), despite their divergence at low frequencies (around 1 Hz). The same tendency can be clearly observed in Figure 6.

Comparison of the Vertical and Horizontal Coda Quality Factors

As already mentioned, vertical and horizontal coda quality factor functions in this study are estimated from the vertical and horizontal components of seismograms, respectively. To investigate the difference between Q_C^V and Q_C^H, the corresponding Q_0 and η for different coda window lengths are plotted in Figure 7. Based on Figure 7, Q_0^V values are greater than Q_0^H values at all coda window lengths, which indicate that attenuation for the vertical component is lower than for the horizontal component. In addition, η values are slightly lower for the vertical component than for the horizontal component. This may imply that seismic waves encounter less attenuation in the vertical direction than in the horizontal direction, and the degree of vertical heterogeneities is less than the degree of lateral heterogeneities.

Area Covered by the Estimated Coda Quality Factors and Variation of Attenuation with Depth

The coda quality factor represents the average attenuation property of an ellipsoidal volume with the source and receiver as its focus and depth as its height. Shengelia *et al.* (2011) computed the penetration depth and covered area to be 56 km and 7071 km^2 for their proposed coda quality factor function (station ONI), in which the coda window length is 40 s. Ma'hood and Hamzehloo (2009) calculated the penetration depth and covered area equal to 65 km and 13,000 km^2 for their presented coda quality factor in which the coda window length is 40 s. Padhy *et al.* (2011) estimated penetration depths to be 37.7, 172, and 150.8 km for different stations with a coda window length of 40 s. In the study of Kumar *et al.* (2005), the authors estimated the penetration depth to be in the range of 77 to 188 km. Hence, we should mention that penetration depths and covered areas depend on the database used in the analysis, because the average focal depth and average hypocentral distance can vary based on records in the database. In this study, the penetration depth of the estimated coda Q factors and covered area for each station are determined using equations (9)–(11), assuming $V_S = 3.58$ km/s (Dreiling *et al.*, 2014), $h_{\mathrm{avg}} = 9$ km, and $\Delta = 64$ km. Because the average values of focal depths and epicentral distances for all stations are fairly close, the mentioned values in Table 5 are applicable for all stations. As Table 5 shows, Q_C increases as the length of the coda window increases. Increasing the coda window length can be interpreted as increasing the depth in which the average coda quality factor is evaluated. The average crust thickness in the NMSZ is about 40 km and the thickness of the upper mantle ranges from 50 to 140 km (Zhang *et al.*, 2009; Pollitz and Walter, 2014). Hence, based on the computed penetration depths, coda quality factors estimated from all considered coda window lengths in this study sample characteristics of the crust and upper mantle. Of course, a coda window length of 20 s mostly reflects attenuation characteristics of the crust because the penetration depth for this length is about 48 km, whereas a coda window length of 60 s reflects the combined effect from the crust and upper mantle because the penetration depth goes down to 89 km. This indicates that with increasing depth, the heterogeneity level of the Earth's crust and upper mantle decreases because the attenuation and scatter rate of the seismic waves are reduced. Accordingly, the lower lithosphere is more homogeneous and stable in comparison with the upper lithosphere. Furthermore, the area covered by the estimated coda quality factor augments as the length of the coda window augments. Hence, once the coda window length increases, the calculated Q_C provides the average of the quality factor for a larger sampling volume. Finally, the coda quality factor function for a specific place located in the NMSZ can be obtained using Table 5 according to the desired penetration depth and covered area.

Comparison of Results with Previous Studies for the NMSZ

An applicable estimation of Q_0 and η has been provided by Baqer and Mitchell (1998) for the continental United States. Baqer and Mitchell (1998) used a stacked ratio method (Xie and Nuttli, 1988) and the Lg phase of records. The dataset used in Baqer and Mitchell (1998) consists of

Table 3
Average Vertical Quality Factor Values at Each Frequency Band Obtained from Local Earthquakes in the New Madrid Seismic Zone (NMSZ)

Coda Window Length	Station	1.5	3	6	12	24	$Q_C^V(f) = Q_0 f^\eta$
20 s	GLAT	730.81	747.89	1130.23	1900.42	3286.88	$Q = 473.18f^{0.568}$
	GNAR	531.55	709.94	849.07	1966.18	3404.55	$Q = 342.73f^{0.683}$
	HALT	544.50	791.34	1459.28	2298.49	3150.29	$Q = 414.78f^{0.660}$
	HBAR	406.81	880.01	1424.66	1908.20	3099.14	$Q = 357.34f^{0.698}$
	HENM	536.45	742.22	909.88	1795.27	3192.24	$Q = 366.31f^{0.642}$
	HICK	424.86	663.20	1170.94	2171.75	3006.92	$Q = 311.97f^{0.736}$
	LNXT	630.41	779.41	1358.49	2034.04	3187.57	$Q = 452.60f^{0.607}$
	LPAR	506.54	525.53	1322.80	2269.29	3331.05	$Q = 314.72f^{0.754}$
	PARM	737.24	903.55	1169.76	2203.01	3245.14	$Q = 520.44f^{0.556}$
	PEBM	643.86	629.79	1120.37	2144.24	3208.21	$Q = 398.88f^{0.640}$
	PENM	363.62	752.06	933.78	2083.25	3310.33	$Q = 274.70f^{0.784}$
	Whole Area	558.58	738.60	1150.07	2076.59	3214.62	$Q = 390.08f^{0.654}$
30 s	GLAT	772.01	747.10	1265.35	2081.48	3107.78	$Q = 509.42f^{0.550}$
	GNAR	738.16	906.39	1284.00	2233.51	3685.12	$Q = 510.07f^{0.594}$
	HALT	911.59	1011.27	1574.54	2338.07	3512.96	$Q = 658.09f^{0.510}$
	HBAR	408.54	667.05	1216.40	2038.63	3201.11	$Q = 301.56f^{0.755}$
	HENM	769.09	791.61	1167.19	2159.49	3265.12	$Q = 504.29f^{0.562}$
	HICK	769.82	733.88	1156.02	2366.05	3410.62	$Q = 477.24f^{0.598}$
	LNXT	833.67	742.57	1398.18	2276.58	3356.97	$Q = 531.59f^{0.564}$
	LPAR	444.64	553.15	1366.07	2519.85	3642.22	$Q = 285.35f^{0.823}$
	PARM	453.15	897.82	1509.00	2269.46	3484.06	$Q = 598.29f^{0.537}$
	PEBM	700.71	1128.70	1193.80	2668.01	3574.05	$Q = 535.14f^{0.594}$
	PENM	791.86	1003.52	1157.01	1924.37	3896.07	$Q = 545.56f^{0.554}$
	Whole Area	698.68	829.12	1300.71	2248.21	3476.74	$Q = 480.55f^{0.607}$
40 s	GLAT	1130.74	783.45	1625.71	2345.53	3278.45	$Q = 702.66f^{0.465}$
	GNAR	948.89	814.60	1505.36	2341.21	3763.79	$Q = 594.67f^{0.550}$
	HALT	909.91	1012.20	1802.84	2428.72	3565.30	$Q = 670.89f^{0.520}$
	HBAR	746.63	749.99	1420.75	2016.63	3165.55	$Q = 507.89f^{0.559}$
	HENM	1190.75	1157.04	1229.28	2276.10	3259.84	$Q = 827.49f^{0.388}$
	HICK	791.61	693.59	1403.87	2378.14	3434.30	$Q = 492.01f^{0.601}$
	LNXT	943.22	961.69	1601.20	2303.37	3319.59	$Q = 673.79f^{0.489}$
	LPAR	733.92	832.73	1512.30	2404.23	3602.71	$Q = 506.30f^{0.612}$
	PARM	453.29	1047.82	1482.88	2228.39	3592.74	$Q = 398.77f^{0.706}$
	PEBM	970.20	737.97	1375.59	2263.34	3803.32	$Q = 566.38f^{0.556}$
	PENM	1186.81	1097.70	1437.42	1935.38	3755.86	$Q = 802.51f^{0.414}$
	Whole Area	880.05	881.33	1499.26	2280.03	3507.40	$Q = 597.77f^{0.536}$
50 s	GLAT	879.83	904.79	1749.63	2416.16	3546.32	$Q = 619.60f^{0.544}$
	GNAR	842.60	772.94	1706.69	2590.53	3732.54	$Q = 544.89f^{0.604}$
	HALT	762.25	1555.48	1971.42	2469.63	3609.94	$Q = 728.95f^{0.515}$
	HBAR	809.50	790.71	1666.53	2163.37	3201.81	$Q = 564.91f^{0.542}$
	HENM	921.91	948.96	1427.36	2282.14	3299.11	$Q = 645.45f^{0.494}$
	HICK	921.15	741.55	1446.03	2393.85	3482.55	$Q = 566.19f^{0.553}$
	LNXT	1284.52	1147.31	1698.81	2347.88	3562.13	$Q = 901.12f^{0.399}$
	LPAR	756.22	830.71	1610.70	2390.10	3383.53	$Q = 533.97f^{0.585}$
	PARM	1117.25	959.49	1775.68	2235.69	3600.29	$Q = 757.46f^{0.460}$
	PEBM	888.35	927.15	1531.32	2372.52	4031.85	$Q = 590.46f^{0.572}$
	PENM	993.21	1064.80	1288.29	1987.89	3702.01	$Q = 638.49f^{0.470}$
	Whole Area	949.33	941.56	1628.70	2339.29	3577.52	$Q = 656.31f^{0.514}$
60 s	GLAT	1125.88	1013.45	1761.17	2404.32	3592.82	$Q = 776.93f^{0.459}$
	GNAR	920.53	823.81	1563.53	2490.00	3763.96	$Q = 587.20f^{0.566}$
	HALT	908.41	1387.08	2041.04	2502.07	3632.90	$Q = 787.62f^{0.485}$
	HBAR	594.17	871.93	1635.20	2274.19	3274.91	$Q = 466.80f^{0.631}$
	HENM	757.93	872.48	1521.75	2280.42	3288.01	$Q = 547.26f^{0.562}$
	HICK	786.29	965.53	1734.59	2516.03	3457.72	$Q = 591.22f^{0.566}$
	LNXT	914.57	1314.25	1694.63	2380.09	3543.71	$Q = 751.99f^{0.476}$
	LPAR	867.65	843.45	1640.74	2357.35	3344.27	$Q = 598.29f^{0.538}$
	PARM	1329.66	862.51	1675.22	2256.08	3627.15	$Q = 805.43f^{0.428}$
	PEBM	1051.04	821.16	1620.88	2428.98	3851.65	$Q = 645.68f^{0.531}$
	PENM	1103.86	1313.01	1450.70	2029.34	3826.21	$Q = 821.47f^{0.421}$
	Whole Area	966.14	1008.26	1683.16	2361.73	3587.60	$Q = 689.38f^{0.501}$

Table 4
Average Horizontal Quality Factor Values at Each Frequency Band Obtained from Local Earthquakes in the New Madrid Seismic Zone (NMSZ)

Coda Window Length	Station	1.5	3	6	12	24	$Q_C^H(f) = Q_0 f^{\eta}$
20 s	GLAT	412.63	599.68	1027.78	1739.62	2781.44	$Q = 295.14f^{0.704}$
	GNAR	460.81	553.04	916.71	1828.17	3385.26	$Q = 281.86f^{0.748}$
	HALT	460.05	784.69	1224.81	2340.93	3293.11	$Q = 348.24f^{0.726}$
	HBAR	363.79	507.80	1016.60	1939.07	2873.32	$Q = 245.19f^{0.790}$
	HENM	606.14	910.38	1115.16	2027.45	2984.73	$Q = 463.85f^{0.575}$
	HICK	593.16	610.75	1026.00	1885.40	2987.23	$Q = 375.53f^{0.629}$
	LNXT	677.95	753.65	1253.86	2853.31	3203.83	$Q = 452.24f^{0.640}$
	LPAR	349.07	558.88	1334.17	2422.74	3361.15	$Q = 246.65f^{0.865}$
	PARM	446.82	1098.20	1293.63	2479.64	3383.78	$Q = 397.44f^{0.701}$
	PEBM	723.42	1016.06	1125.11	2399.10	3225.97	$Q = 535.94f^{0.555}$
	PENM	677.66	828.44	961.96	1965.35	3546.63	$Q = 443.13f^{0.602}$
	Whole Area	528.47	753.66	1115.02	2150.63	3184.55	$Q = 376.38f^{0.669}$
30 s	GLAT	561.97	724.36	1216.99	1894.89	2963.41	$Q = 405.14f^{0.619}$
	GNAR	597.47	675.90	1303.03	2159.21	3243.71	$Q = 400.92f^{0.656}$
	HALT	781.42	820.32	1621.96	2455.33	3464.34	$Q = 539.37f^{0.588}$
	HBAR	435.58	576.60	1049.11	2132.94	3225.74	$Q = 285.27f^{0.766}$
	HENM	544.16	790.90	1215.94	2381.35	3263.99	$Q = 394.35f^{0.677}$
	HICK	579.68	621.35	1200.58	2238.33	3180.08	$Q = 372.90f^{0.676}$
	LNXT	732.32	929.84	1312.87	2137.48	3299.40	$Q = 535.19f^{0.554}$
	LPAR	369.94	969.44	1670.98	2636.85	3342.68	$Q = 345.14f^{0.779}$
	PARM	769.13	964.68	1293.69	2505.04	3451.52	$Q = 549.02f^{0.571}$
	PEBM	755.64	981.28	1544.32	2639.55	3643.43	$Q = 554.73f^{0.600}$
	PENM	736.51	658.19	1075.28	2029.20	3618.10	$Q = 429.12f^{0.622}$
	Whole Area	634.61	789.38	1307.76	2275.55	3330.85	$Q = 444.70f^{0.631}$
40 s	GLAT	662.23	721.39	1511.28	2157.60	3249.60	$Q = 457.85f^{0.617}$
	GNAR	827.87	802.33	1578.37	2367.92	3495.52	$Q = 553.06f^{0.571}$
	HALT	926.38	1036.16	1834.31	2648.98	3622.66	$Q = 682.33f^{0.523}$
	HBAR	647.67	731.05	1390.59	2320.13	3369.85	$Q = 438.90f^{0.642}$
	HENM	640.12	859.09	1294.34	2376.38	3278.16	$Q = 465.39f^{0.618}$
	HICK	592.65	706.44	1369.53	2322.73	3275.48	$Q = 407.81f^{0.665}$
	LNXT	654.00	875.50	1719.61	2340.10	3421.59	$Q = 498.23f^{0.619}$
	LPAR	761.56	868.29	1695.53	2523.74	3161.02	$Q = 563.58f^{0.564}$
	PARM	846.83	974.51	1478.91	2626.23	3555.45	$Q = 599.67f^{0.557}$
	PEBM	522.03	763.76	1471.28	2690.71	3781.28	$Q = 370.86f^{0.753}$
	PENM	1043.84	655.96	1079.32	1942.94	3595.07	$Q = 553.34f^{0.513}$
	Whole Area	731.27	823.64	1487.72	2378.98	3440.46	$Q = 508.50f^{0.600}$
50 s	GLAT	764.71	829.94	1643.08	2324.19	3400.69	$Q = 540.20f^{0.579}$
	GNAR	931.07	911.32	1657.76	2618.89	3605.02	$Q = 643.13f^{0.543}$
	HALT	956.24	1080.96	1978.87	2420.72	3639.80	$Q = 725.32f^{0.502}$
	HBAR	847.01	854.79	1514.35	2316.28	3433.00	$Q = 578.03f^{0.548}$
	HENM	689.71	943.79	1582.48	2433.77	3334.50	$Q = 530.00f^{0.591}$
	HICK	542.06	765.11	1595.64	2328.94	3278.13	$Q = 408.94f^{0.680}$
	LNXT	682.69	852.20	1763.28	2343.10	3419.23	$Q = 510.11f^{0.611}$
	LPAR	650.92	899.36	1664.94	2515.60	3023.10	$Q = 517.27f^{0.591}$
	PARM	943.41	1037.51	1667.04	2533.28	3543.57	$Q = 685.16f^{0.511}$
	PEBM	740.49	785.43	1858.32	2632.14	3690.53	$Q = 510.29f^{0.640}$
	PENM	1012.93	891.74	1429.14	1997.25	3508.53	$Q = 663.47f^{0.475}$
	Whole Area	771.58	896.19	1667.24	2399.06	3450.71	$Q = 561.15f^{0.574}$
60 s	GLAT	906.70	960.30	1742.64	2334.80	3546.50	$Q = 651.40f^{0.522}$
	GNAR	932.87	946.74	1808.83	2607.85	3567.67	$Q = 659.91f^{0.533}$
	HALT	1115.98	1110.14	2096.13	2918.83	3753.78	$Q = 812.72f^{0.489}$
	HBAR	835.32	1205.23	1620.85	2405.19	3351.13	$Q = 682.82f^{0.500}$
	HENM	846.25	1038.15	1618.48	2495.41	3310.36	$Q = 644.56f^{0.520}$
	HICK	667.74	951.32	1740.22	2336.61	3659.09	$Q = 515.56f^{0.620}$
	LNXT	801.66	835.52	1749.80	2433.75	3576.25	$Q = 557.11f^{0.585}$
	LPAR	646.05	1110.82	1716.07	2494.64	3026.87	$Q = 570.26f^{0.562}$
	PARM	1227.20	998.20	1654.94	2541.79	3408.75	$Q = 821.52f^{0.430}$
	PEBM	1446.20	737.67	2122.55	2733.38	3726.43	$Q = 818.50f^{0.462}$
	PENM	1045.89	828.26	1385.61	2086.98	3372.94	$Q = 658.73f^{0.471}$
	Whole Area	895.75	961.29	1742.87	2473.81	3515.60	$Q = 645.67f^{0.531}$

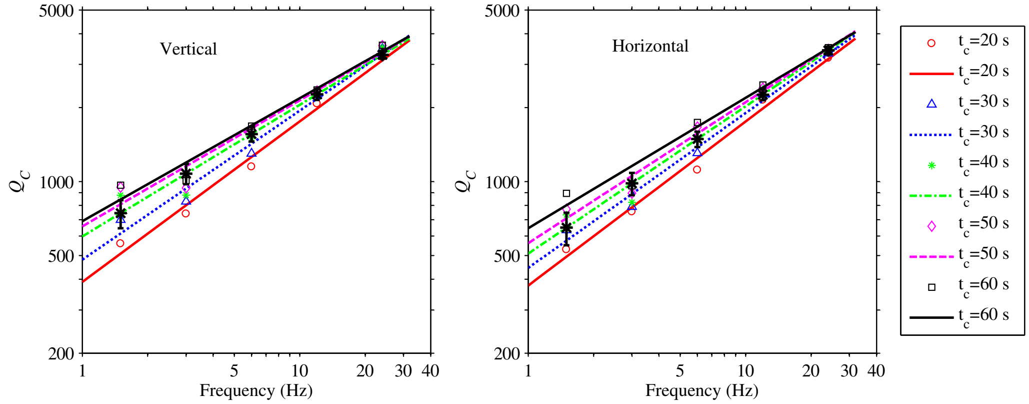

Figure 6. Vertical and horizontal Q_C values as well as fitted lines versus frequencies for different coda window lengths. Dots and lines show estimated values and fitted lines, respectively. Vertical black lines demonstrate error bars for the estimated coda quality factor function with the coda window length of 40 s. The color version of this figure is available only in the electronic edition.

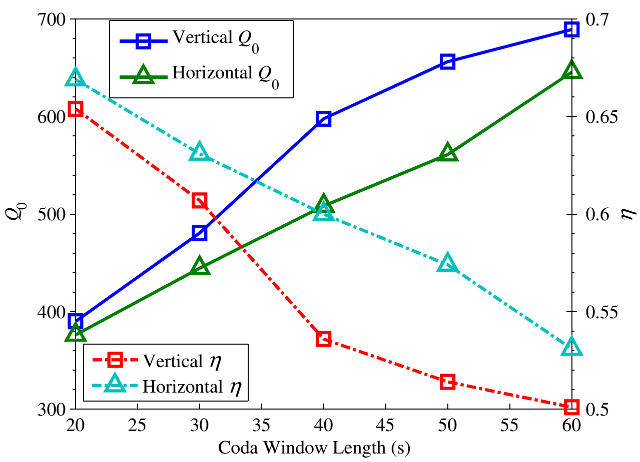

Figure 7. Q_0 and η values versus the length of coda window. The color version of this figure is available only in the electronic edition.

218 vertical-component records from 108 regional seismic events that occurred in the period of 1981–1996. In the study of Baqer and Mitchell (1998), the Gulf Coast region has a Q_0 range of 350 (southern part) to 600 (northern part). The NMSZ is placed at the northern part of the Gulf Coast region; therefore, according to the regional variation of Q_{Lg} maps provided by Baqer and Mitchell (1998), Q_0 and η values vary from 500 to 600 and 0.5 to 0.6, respectively, in the NMSZ. To compare results, we use a length of 40 s for the coda window because estimated coda quality factors for this coda window length approximately represent the average quality factor values estimated from all window lengths at each center frequency. We evaluated $Q_C^V = 598f^{0.54}$ and $Q_C^H = 509f^{0.60}$ for vertical and horizontal components for a coda window length of 40 s. In conclusion, it can be said that Q_C values correlate well with the amounts of Q_{Lg} estimated from *Lg* waves. The same conclusion has been previously made by Singh and Herrmann (1983).

Zandieh and Pezeshk (2010) estimated $Q = 614f^{0.32}$ for vertical components and frequencies greater than 1 Hz and we derived $Q_C^V = 598f^{0.54}$ for vertical components with a coda window length of 40 s. Q_0 values of these functions are close; however, the values of the frequency-dependent power η are distinct. One reason why η values are different may be attributed to using different procedures and different geometrical spreading functions to acquire the quality factor. Zandieh and Pezeshk (2010) used body waves to estimate Q factor, whereas we used the coda portion of seismograms in this study to obtain the coda Q factor. As mentioned earlier, coda waves are considered as backscattered body waves from randomly distributed heterogeneities in the Earth's crust and upper mantle. Hence, the larger value of η for the coda Q factor may result from the direct influence of the high heterogeneity level (Langston, 2003) of the Earth's crust and the upper mantle in the NMSZ on coda waves. Another reason for the discrepancy for η values may be derived from the difference between the datasets. Hypocentral distances of local events range from 10 to 400 km for Zandieh and Pezeshk (2010), whereas hypocentral distances of local earthquakes used in this study range from 10 to 200 km. Therefore, the evaluated quality factor in the study of Zandieh and Pezeshk (2010) samples more regions that are mostly considered stable areas around the NMSZ. Consequently, the estimated quality factor could be easily affected by the range of hypocentral distances. Of course, this issue can also explain why the Q_0 value from Zandieh and Pezeshk (2010) is slightly greater than the estimated Q_0 in this study.

The comparison of Q factor parameters originated from body, coda, and *Lg* waves reveals there is not much difference between them (Modiano and Hatzfeld, 1982; Al-Shukri *et al.*, 1988).

Comparison of Results with Other Regions

To reasonably compare the results acquired in this study with the coda qualify factor functions reported by other investigators from local earthquakes in various regions, it is more appropriate to have similar coda window lengths. Therefore, coda Q factor functions with a length of 40 as the coda

Table 5
Penetration Depth and Coverage of the Area for the Estimated Q_C Functions Obtained from Local Earthquakes in the New Madrid Seismic Zone (NMSZ)

Coda Window Length (s)	Q_C^V	Q_C^H	Penetration Depth (km)	Covered Area (km^2)
20	$(390.08 \pm 35.76)f^{(0.654\pm0.043)}$	$(376.38 \pm 33.80)f^{(0.669\pm0.042)}$	48	6,192
30	$(480.55 \pm 56.91)f^{(0.607\pm0.055)}$	$(444.70 \pm 44.28)f^{(0.631\pm0.046)}$	59	9,343
40	$(597.77 \pm 94.90)f^{(0.536\pm0.072)}$	$(508.50 \pm 63.91)f^{(0.600\pm0.058)}$	70	12,968
50	$(656.31 \pm 101.47)f^{(0.514\pm0.070)}$	$(561.15 \pm 62.17)f^{(0.574\pm0.051)}$	80	17,082
60	$(689.38 \pm 88.59)f^{(0.501\pm0.059)}$	$(645.67 \pm 81.88)f^{(0.531\pm0.059)}$	89	21,692

The term after ± represents one standard error.

Table 6
Parameters of the Selected Coda Quality Factor Functions for Vertical Components

Number	Seismicity	Region	Source	Q	η	Coda Window Length (s)
1	Active	Washington, United States	Havskov *et al.* (1989)	63	0.97	20
2	Active	Parkfield, California, United States	Hellweg *et al.* (1995)	79	0.74	30
3	Active	Zagros, Iran	Rahimi and Hamzehloo (2008)	88	0.90	40
4	Active	Charlevoix, Quebec, Canada	Woodgold (1994)	91	0.95	20–40
5	Moderate	New England, United States	Pulli (1984)	460	0.40	<100
6	Moderate	South Indian Peninsular Shield	Kumar *et al.* (2005)	535	0.59	40
7	Moderate	This study	–	598	0.54	40
8	Stable	NW Iberia	Pujades *et al.* (1990)	600	0.45	20<
9	Stable	Northeast United States	Singh and Herrmann (1983)	900	0.35	–
10	Stable	Central United States	Singh and Herrmann (1983)	1000	0.20	–

window have been considered for consistency, if they were available. For tectonically active areas, low Q_0 values and high values of the frequency-dependent power η ($Q_0 < 200$, $\eta > 0.7$) have been reported (Aki and Chouet, 1975; Havskov *et al.*, 1989; Woodgold, 1994; Hellweg *et al.*, 1995; Giampiccolo *et al.*, 2004; Rahimi and Hamzehloo, 2008; Padhy *et al.*, 2011; Shengelia *et al.*, 2011; Sertçelik, 2012; de Lorenzo *et al.*, 2013; Ma'hood, 2014; Farrokhi *et al.*, 2015). On the other hand, for tectonically inactive areas, high Q_0 values and low values of the frequency-dependent power η ($Q_0 > 600$, $\eta < 0.4$) have been acquired (Singh and Herrmann, 1983; Hasegawa, 1985; Pujades *et al.*, 1990; Atkinson and Mereu, 1992; Atkinson, 2004). Finally, moderate values of Q_0 and η ($200 < Q < 600$, $0.4 < \eta < 0.7$) have been obtained for regions between active and inactive areas considered as moderately active regions (Roecker *et al.*, 1982; Pulli, 1984; Patanjali Kumar *et al.*, 2007). Table 6 presents Q_0 and η values for the selected studies, and Figure 8 shows the Q-factor function evaluated in this study in comparison with chosen Q-factor functions from the other regions. Referring to Figure 8, there are equivalent trends for regions with similar tectonic activities and the NMSZ obviously follows the trend for regions with moderate seismic activities. It is worth noting that all of these coda quality functions have been estimated using local earthquakes.

Geometrical Spreading

In this study, the horizontal component of the coda quality factor computed for a time window with a length of 40 s has been considered to estimate the geometrical spreading. To estimate the geometrical spreading, 160 seismograms with distances less than 60 km have been considered. We also estimated geometrical spreading factors using quality factor functions proposed by Zandieh and Pezeshk (2010), instead of Q_C computed in this study, and found that the difference between results is less than 3%. Figure 9 illustrates the distribution of the natural logarithm of the ratio of the S-wave to coda-wave amplitudes times the attenuation factor versus the hypocentral distance for a time window with a length of 40 s centered at 80 s after the origin time. Plus, the fitted line representing the geometrical spreading decay has been displayed at each center frequency. Table 7 tabulates all of the geometrical spreading functions corresponding to different coda time windows. In this study, the geometrical spreading factor decreases when the frequency increases for frequencies greater than or equal to 6 Hz, whereas it increases with increasing frequency for frequencies less than 6 Hz. Frankel (2015) clarifies that the estimated geometrical spreading functions for low frequencies may be attributed to the radiation pattern and rupture directivity, because the impact of the radiation pattern and rupture directivity increases by decreasing the frequency. Plus, the contribution of low frequencies in the frequency content of a small ground motion is less than the contribution of high frequencies. Therefore, band-pass-filtered seismograms of small earthquakes are very sensitive to the noise at low frequencies and using them may lead to unstable results. As can be seen from Table 7, the effect of the time-window length and location is very significant at lower frequencies because

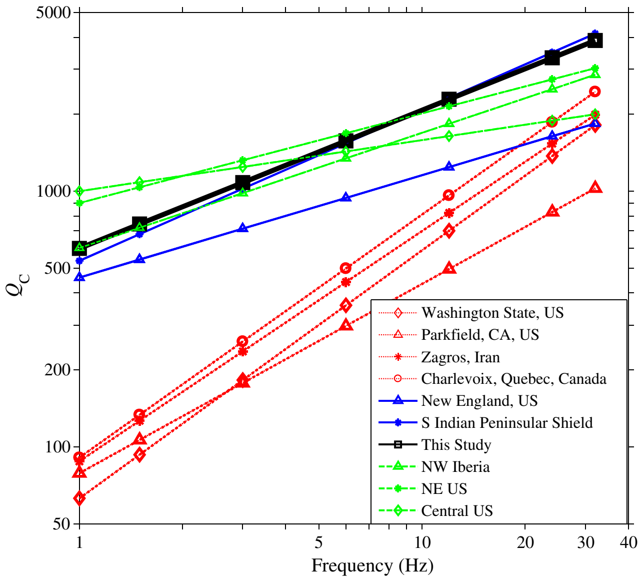

Figure 8. Comparison of the selected vertical coda Q-factor functions. The color version of this figure is available only in the electronic edition.

the database contains many noisy records, and low-frequency band-pass-filtered seismograms are very sensitive to background noise. However, for a frequency greater than 3 Hz, the time-window length and location do not affect the estimated geometrical factor. Based on these two reasons, the estimated geometrical spreading factors for low frequencies may not be appropriate to be applied in simulating time series.

Summary and Conclusions

According to the history of earthquake activities in the NMSZ, this region has a high potential to generate a very large earthquake. In addition, this region possesses unique and different attenuation characteristics in comparison with other regions of CENA. The estimation of the quality factor and the geometrical spreading is essential to develop GMMs and perform seismic-hazard assessment.

The single backscattering theory has been applied to estimate the quality factor for coda waves. In this study, Q_C^V and Q_C^H for vertical and horizontal directions have been determined for the stations and the whole region of the NMSZ, using 284 triaxial seismograms from 57 local earthquakes provided by CERI at the University of Memphis, in five frequency bands through five various coda window lengths. Next, the coda normalization technique has been applied to evaluate the geometrical spreading for the geometric mean of horizontal components, using 160 seismograms from 284 initial triaxial seismograms recorded within hypocentral distances less than 60 km.

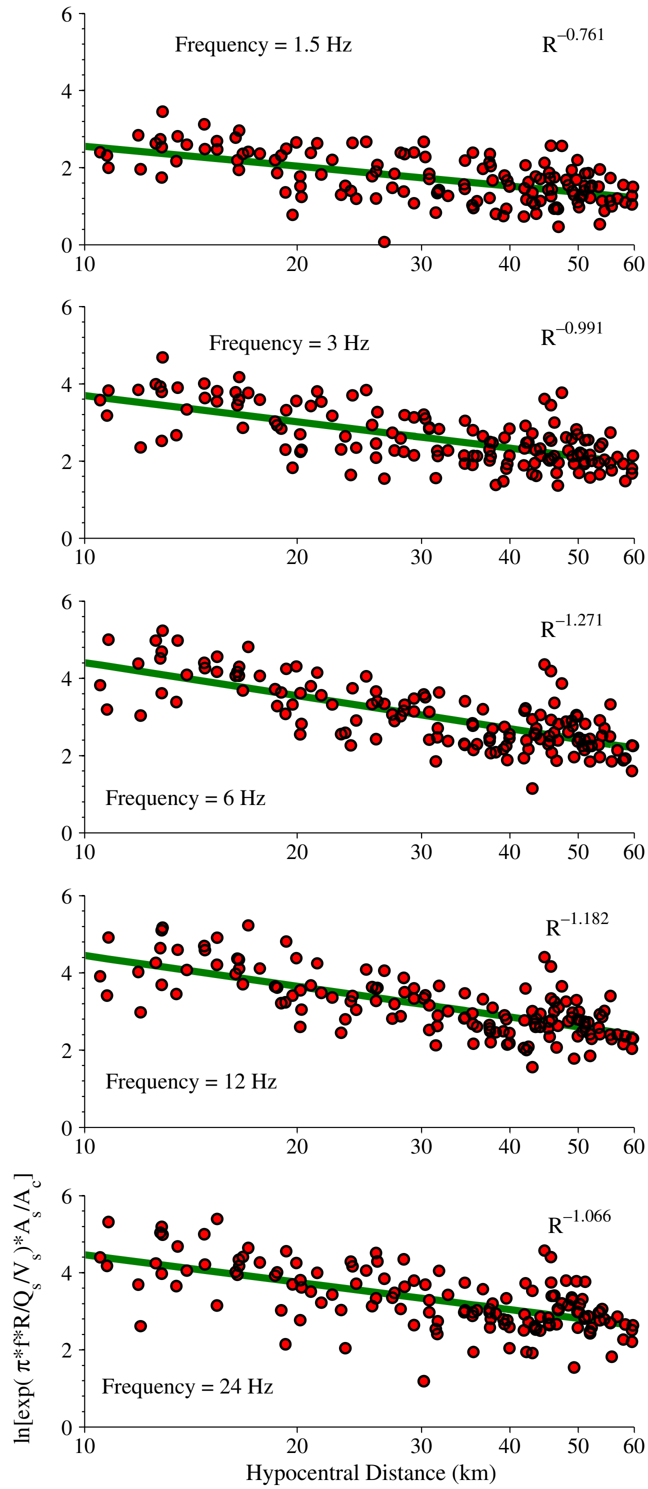

Figure 9. Estimated geometrical spreading functions for the geometric average of the horizontal components with the coda window length of 40 s centered at 80 s. The color version of this figure is available only in the electronic edition.

- $Q_C^V = (597.77 \pm 94.90) f^{(0.536\pm0.072)}$ and $Q_C^H = (508.50 \pm 63.91) f^{(0.600\pm0.058)}$ for vertical and horizontal directions with a coda window length of 40 s in which the penetration depth is 70 km and the covered area is 12,968 km^2.
- There is a slight difference between coda quality factor functions estimated from vertical and horizontal compo-

Table 7
Horizontal Geometrical Spreading Factors for Different Coda Time Windows

		Central Frequency (Hz)				
t_C (s)	Length (s)	1.5	3	6	12	24
60	5	0.674 ± 0.104	0.898 ± 0.078	1.278 ± 0.095	1.152 ± 0.039	1.097 ± 0.090
70	5	0.730 ± 0.101	0.975 ± 0.150	1.258 ± 0.086	1.198 ± 0.062	1.100 ± 0.063
80	5	0.800 ± 0.136	1.041 ± 0.144	1.276 ± 0.062	1.167 ± 0.056	1.060 ± 0.117
90	5	0.891 ± 0.101	1.025 ± 0.119	1.269 ± 0.079	1.189 ± 0.064	1.069 ± 0.139
97.5	5	0.879 ± 0.113	1.078 ± 0.098	1.294 ± 0.076	1.209 ± 0.053	1.058 ± 0.071
80	40	0.761 ± 0.102	0.991 ± 0.109	1.271 ± 0.060	1.182 ± 0.089	1.066 ± 0.062

The term after ± represents one standard error.

nents. Estimated quality factor functions demonstrate that seismic waves encounter more heterogeneities and more attenuation in the horizontal direction than in the vertical direction. This interpretation suggests that to model the layered structures of the crust and upper mantle in the NMSZ, the degree of lateral heterogeneities should be slightly larger than the degree of vertical heterogeneities.

- The Earth's crust and upper mantle beneath the NMSZ is considered to be a tectonically moderate region with a moderate to relatively high level of heterogeneity.
- By increasing the depth (the length of the coda window), the Earth's crust and upper mantle in the NMSZ become more homogenous.
- Q-factor functions estimated from various phases of seismograms, such as shear waves, coda waves, and Lg waves, do not significantly differ.
- The values of Q_0 and η are well correlated with values reported by other investigators for regions with moderate seismic activities.
- In this study, the geometrical spreading is found to be frequency dependent. $R^{-0.761\pm0.102}$, $R^{-0.991\pm0.109}$, $R^{-1.271\pm0.060}$, $R^{-1.182\pm0.089}$, and $R^{-1.066\pm0.062}$ are the estimated geometrical spreading functions from the geometric average of horizontal components at central frequencies of 1.5, 3, 6, 12, and 24 Hz at hypocentral distances less than 60 km.
- The obtained geometrical spreading functions at center frequencies of 1.5 and 3 Hz may not be appropriate for simulating time histories to be used for GMMs or GMPEs, because they are not stable due to the sensitivity to the background noise as well as the effect of the radiation pattern and rupture directivity.
- For frequencies greater than or equal to 6 Hz, results acquired through coda time windows with different lengths centered at various lapse times from origin times, which are greater than the twice shear-wave arrivals, show no difference. This implies that the decay rates of the coda phase for the envelopes of seismograms are similar at different lapse times.

Data and Resources

Digital waveform seismograms considered in this study were collected as part of the Advanced National Seismic System (ANSS) for the central and eastern United States (CEUS). Data can be acquired through the ANSS at http://earthquake.usgs.gov/monitoring/anss/regions/mid/ (last accessed April 2010).

Figure 2 was made using the Generic Mapping Tools v.4.5.13 (Wessel and Smith, 1998).

Acknowledgments

We express our sincere appreciation to Mitch Withers for providing us the Center for Earthquake Research and Information (CERI) broadband seismograms. The authors would also like to thank Arash Zandieh, Mostafa Mousavi, Ann Meier, Naeem Khoshnevis, and anonymous reviewers for their thoughtful comments and constructive suggestions that significantly improved this article. This project was partially supported by the Tennessee Department of Transportation.

References

Aagaard, B. T., T. M. Brocher, D. Dreger, R. W. Graves, S. Harmsen, S. Hartzell, S. Larsen, K. McCandless, S. Nilsson, N. A. Petersson, *et al.* (2008). Ground-motion modeling of the 1906 San Francisco earthquake, part II: Ground-motion estimates for the 1906 earthquake and scenario events, *Bull. Seismol. Soc. Am.* **98,** 1012–1046.

Abercrombie, R. E. (1995). Earthquake source scaling relationships from −1 to 5 M L using seismograms recorded at 2.5 km depth, *J. Geophys. Res.* **100,** 24,015–24,036.

Abercrombie, R. E., and P. Leary (1993). Source parameters of small earthquakes recorded at 2.5 km depth, Cajon Pass, southern California: Implications for earthquake scaling, *Geophys. Res. Lett.* **20,** 1511–1514.

Aki, K. (1969). Analysis of the seismic coda of local earthquakes as scattered waves, *J. Geophys. Res.* **74,** 615–631.

Aki, K. (1980a). Attenuation of shear-waves in the lithosphere for frequencies from 0.05 to 25 Hz, *Phys. Earth Planet. In.* **21,** 50–60.

Aki, K. (1980b). Scattering and attenuation of shear waves in the lithosphere, *J. Geophys. Res.* **85,** 6496–6504.

Aki, K, and B. Chouet (1975). Origin of coda waves: Source, attenuation, and scattering effects, *J. Geophys. Res.* **80,** 3322–3342.

Al-Shukri, H. J., B. J. Mitchell, and A. A. Ghalib (1988). Attenuation of seismic waves in the New Madrid seismic zone, *Seismol. Res. Lett.* **59,** 133–140.

Anderson, J. G., and S. E. Hough (1984). A model for the shape of the Fourier amplitude spectrum of acceleration at high frequencies, *Bull. Seismol. Soc. Am.* **74,** 1969–1993.

Atkinson, G. M. (2004). Empirical attenuation of ground motion spectral amplitudes in southeastern Canada and the northeastern United States, *Bull. Seismol. Soc. Am.* **94,** 1079–1095.

Atkinson, G. M., and D. M. Boore (2014). The attenuation of Fourier amplitudes for rock sites in eastern North America, *Bull. Seismol. Soc. Am.* **104,** 513–528.

Atkinson, G. M., and R. Mereu (1992). The shape of ground motion attenuation curves in southeastern Canada, *Bull. Seismol. Soc. Am.* **82,** 2014–2031.

Bakun, W. H., and A. G. Lindh (1977). Local magnitudes, seismic moments, and coda durations for earthquakes near Oroville, California, *Bull. Seismol. Soc. Am.* **67,** 615–629.

Baqer, S., and B. J. Mitchell (1998). Regional variation of L_g coda Q in the continental United States and its relation to crustal structure and evolution, *Pure Appl. Geophys.* **158,** 613–638.

Bonilla, L. F., J. H. Steidl, G. T. Lindley, A. G. Tumarkin, and R. J. Archuleta (1997). Site amplification in the San Fernando Valley, CA: Variability of site effect estimation using the *S*-wave, coda, and H/V methods, *Bull. Seismol. Soc. Am.* 87**,** 710–730.

Boore, D. M. (2003). Prediction of ground motion using the stochastic method, *Pure Appl. Geophys.* **160,** 635–676.

Boore, D. M., and E. M. Thompson (2015). Revisions to some parameters used in stochastic-method simulations of ground motion, *Bull. Seismol. Soc. Am.* **105,** 1029–1041.

Braile, L. W., W. J. Hinze, G. R. Keller, E. G. Lidiak, and J. L. Sexton (1986). Tectonic development of the New Madrid rift complex, Mississippi embayment, North America, *Tectonophysics* **131,** 1–21.

Burger, R., P. Somerville, J. Barker, R. Herrmann, and D. Helmberger (1987). The effect of crustal structure on strong ground motion attenuation relations in eastern North America, *Bull. Seismol. Soc. Am.* **77,** 420–439.

Chapman, M. C., and R. W. Godbee (2012). Modeling geometrical spreading and the relative amplitudes of vertical and horizontal high frequency ground motions in eastern North America, *Bull. Seismol. Soc. Am.* **102,** 1957–1975.

Chen, K., J. Chiu, and Y. Yang (1994). Q_P–Q_S relations in the sedimentary basin of the upper Mississippi embayment using converted phases, *Bull. Seismol. Soc. Am.* **84,** 1861–1868.

Dainty, A. M. (1981). A scattering model to explain seismic Q observations in the lithosphere between 1 and 30 Hz, *Geophys. Res. Lett.* **8,** 1126–1128.

De Lorenzo, S., E. Del Pezzo, and F. Bianco (2013). Q_c, Q_β, Q_i and Q_s attenuation parameters in the Umbria–Marche (Italy) region, *Phys. Earth Planet. In.* **218,** 19–30.

Del Pezzo, E. (2008). Earth heterogeneity and scattering effects on seismic waves, in *Advances in Geophysics*, H. Sato and M. C. Fehler (Editors), Vol. 50, Chapter 13, Academic Press, Elsevier, New York, New York, 353–373.

Del Pezzo, E., R. Allotta, and D. Patane (1990). Dependence of Q_c (coda Q) on coda duration time interval: Model or depth effect?, *Bull. Seismol. Soc. Am.* **80,** 1028–1033.

Dreiling, J., M. P. Isken, W. D. Mooney, M. C. Chapman, and R. W. Godbee (2014). NGA-East regionalization report: Comparison of four crustal regions within central and eastern North America using waveform modeling and 5%-damped pseudo-spectral acceleration response, *PEER Rept.*, 1–230.

Elnashai, A. S., T. Jefferson, F. Fiedrich, L. J. Cleveland, and T. Gress (2009). New Madrid seismic zone catastrophic earthquake response planning project, volume I, impact of New Madrid seismic zone earthquakes on the central USA, *MAE Center Rept. No. 09-03*, 1–139.

Farrokhi, M., H. Hamzehloo, H. Rahimi, and M. Allamehzadeh (2015). Estimation of coda-wave attenuation in the central and eastern Alborz, Iran, *Bull. Seismol. Soc. Am.* **105,** 1756–1767.

Frankel, A. (2015). Decay of *S*-wave amplitudes with distance for earthquakes in the Charlevoix, Quebec, area: Effects of radiation pattern and directivity, *Bull. Seismol. Soc. Am.* **105,** 850–857.

Frankel, A., and L. Wennerberg (1987). Energy-flux model of seismic coda: Separation of scattering and intrinsic attenuation, *Bull. Seismol. Soc. Am.* **77,** 1223–1251.

Frankel, A., A. McGarr, J. Bicknell, J. Mori, L. Seeber, and E. Cranswick (1990). Attenuation of high-frequency shear waves in the crust: Measurements from New York state, South Africa, and southern California, *J. Geophys. Res.* **95,** 17,441–17,457.

Gao, L. S., L. C. Lee, N. N. Biswas, and K. Aki (1983). Comparison of the effects between single and multiple scattering on coda waves for local earthquakes, *Bull. Seismol. Soc. Am.* **73,** 377–389.

Giampiccolo, E., S. Gresta, and F. Rasconà (2004). Intrinsic and scattering attenuation from observed seismic codas in southeastern Sicily (Italy), *Phys. Earth Planet. In.* **145,** 55–66.

Hasegawa, H. S. (1985). Attenuation of L_g waves in the Canadian Shield, *Bull. Seismol. Soc. Am.* **75,** 1569–1582.

Havskov, J., and L. Ottemöller (2005). *SEISAN (version 8.1): The Earthquake Analysis Software for Windows, Solaris, Linux, and Mac OSX Version 8*, 1–254.

Havskov, J., S. Malone, D. Mcclurg, and R. Crosson (1989). Coda Q for the state of Washington, *Bull. Seismol. Soc. Am.* **79,** 1024–1038.

Hellweg, M., P. Spudich, J. B. Fletcher, and L. M. Baker (1995). Stability of coda Q in the region of Parkfield, California: View from the U.S. Geological Survey Parkfield Dense Seismograph Array, *J. Geophys. Res.* **100,** 2089–2102.

Herrmann, R. (1975). The use of duration as a measure of seismic moment and magnitude, *Bull. Seismol. Soc. Am.* **65,** 899–913.

Hosseini, S. M., S. Pezeshk, A. Haji-Soltani, and M. Chapman (2015). Investigation of attenuation of the Fourier amplitude in the Caribbean region, *Bull. Seismol. Soc. Am.* **105,** 686–705.

Jackson, D. D., and D. L. Anderson (1974). Physical mechanism of seismic waves attenuation, *Rev. Geophys. Space Phys.* **8,** 1–63.

Jemberie, A. L., and C. A. Langston (2005). Site amplification, scattering, and intrinsic attenuation in the Mississippi embayment from coda waves, *Bull. Seismol. Soc. Am.* **95,** 1716–1730.

Jin, A., and K. Aki (1988). Spatial and temporal correlation between coda Q and seismicity in China, *Bull. Seismol. Soc. Am.* **78,** 741–769.

Knopoff, L., and J. A. Hudson (1964). Scattering of elastic waves by small inhomogeneities, *J. Acoust. Soc. Am.* **36,** 471–476.

Kopnichev, Y. F. (1977). The role of multiple scattering in the formation of a seismogram's tail, *Phys. Solid Earth* **13,** 394–398.

Kumar, N., I. A. Parvez, and H. S. Virk (2005). Estimation of coda wave attenuation for NW Himalayan region using local earthquakes, *Phys. Earth Planet. In.* **151,** 243–258.

Langston, C. A. (2003). Local earthquake wave propagation through Mississippi embayment sediments, part I: Body-wave phases and local site responses, *Bull. Seismol. Soc. Am.* **93,** 2664–2684.

Liu, L., and M. D. Zoback (1997). Lithospheric strength and intraplate seismicity in the New Madrid seismic zone, *Tectonics* **16,** 585–595.

Liu, Z., M. E. Wuenscher, and R. B. Herrmann (1994). Attenuation of body waves in the central New Madrid seismic zone, *Bull. Seismol. Soc. Am.* **84,** 1112–1122.

Ma'hood, M. (2014). Attenuation of high-frequency seismic waves in eastern Iran, *Pure Appl. Geophys.* **171,** 2225–2240.

Ma'hood, M., and H. Hamzehloo (2009). Estimation of coda wave attenuation in east central Iran, *J. Seismol.* **13,** 125–139.

Mitchell, B. (1995). Anelastic structure and evolution of the continental crust and upper mantle from seismic surface wave attenuation, *Rev. Geophys.* **33,** 441–462.

Modiano, T., and D. Hatzfeld (1982). Experimental study of the spectral content for shallow earthquakes, *Bull. Seismol. Soc. Am.* **72,** 1739–1758.

Montaña, C. A., and G. F. Margrave (2004). Compensating for attenuation by inverse Q filtering, *CREWES Research Rept.* Vol. **16,** 1–20.

Mousavi, S. M., C. H. Cramer, and C. A. Langston (2014). Average Q_{Lg}, Q_{Sn}, and observation of *Lg* blockage in the continental margin of Nova Scotia, *J. Geophys. Res.* **119,** 1–23.

Mukhopadhyay, S., and J. Sharma (2010). Attenuation characteristics of Garwhal–Kumaun Himalayas from analysis of coda of local earthquakes, *J. Seismol.* **14,** 693–713.

Nuttli, O. W. (1973a). Seismic wave attenuation and magnitude relations for eastern North America, *J. Geophys. Res.* **78,** 876–885.

Nuttli, O. W. (1973b). The Mississippi valley earthquakes of 1811 and 1812: Intensities, ground motion, and magnitudes, *Bull. Seismol. Soc. Am.* **63,** 227–248.

Nuttli, O. W., and J. E. Zollweg (1974). The relation between felt area and magnitude for central United States earthquakes, *Bull. Seismol. Soc. Am.* **64,** 73–85.

Padhy, S., N. Subhadra, and J. R. Kayal (2011). Frequency-dependent attenuation of body and coda waves in the Andaman Sea basin, *Bull. Seismol. Soc. Am.* **101,** 109–125.

Patanjali Kumar, C. H., C. S. P. Sarma, M. Shekar, and R. K. Chadha (2007). Attenuation studies based on local earthquake coda waves in the southern Indian peninsular shield, *Nat. Hazards* **40,** 527–536.

Pezeshk, S., A. Zandieh, K. W. Campbell, and B. Tavakoli (2015). Ground motion prediction equations for eastern North America using the hybrid empirical method and NGA-West2 empirical ground motion model, in *NGA-East: Median Ground Motion Models for the Central and Eastern North America Region, Chapter 5, PEER Rept. No. 2015/04*, Pacific Earthquake Engineering Research Center, University of California, Berkeley, California, 119–147.

Polatidis, A., A. Kiratzi, P. Hatzidimitriou, and B. Margaris (2003). Attenuation of shear-waves in the back-arc region of the Hellenic arc for frequencies from 0.6 to 16 Hz, *Tectonophysics* **367,** 29–40.

Pollitz, F. F., and W. D. Walter (2014). Seismic structure of the Central US crust and shallow upper mantle: Uniqueness of the Reelfoot rift, *Earth Planet. Sci. Lett.* **402,** 157–166.

Pujades, L. G., J. A. Canas, J. J. Egozcue, M. A. Puigví, J. Gallart, X. Lana, J. Pous, and A. Casas (1990). Coda-*Q* distribution in the Iberian Peninsula, *Geophys. J. Int.* **100,** 285–301.

Pulli, J. J. (1984). Attenuation of coda waves in New England, *Bull. Seismol. Soc. Am.* **74,** 1149–1166.

Rahimi, H., and H. Hamzehloo (2008). Lapse time and frequency-dependent attenuation of coda waves in the Zagros continental collision zone in southwestern Iran, *J. Geophys. Eng.* **5,** 173–185.

Ramírez-Guzmán, L., R. W. Graves, K. B. Olsen, O. S. Boyd, C. Cramer, S. Hartzell, S. D. Ni, P. Somerville, R. A. Williams, and J. Q. Zhong (2015). Ground motion simulations of 1811–1812 New Madrid earthquakes, central United States, *Bull. Seismol. Soc. Am.* **105,** 1961–1988.

Rautian, T. G., and V. I. Khalturin (1978). The use of the coda for determination of the earthquake source spectrum, *Bull. Seismol. Soc. Am.* **68,** 923–948.

Roecker, S., B. Tucker, J. King, and D. Hatzfeld (1982). Estimates of *Q* in central Asia as a function of frequency and depth using the coda of locally recorded earthquakes, *Bull. Seismol. Soc. Am.* **72,** 129–149.

Ruan, Y. (2012). Surface wave propagation in 3-D anelastic media, *Ph.D. Dissertation*, Virginia Polytechnic Institute and State University, Blacksburg, Virgina.

Samiezade-Yazd, M., R. B. Herrmann, L. Malagnini, and W. Liu (1997). A regional comparison of vertical ground motion in North America, *Rept. No. 1434-94-G-2403*, Saint Louis University, St. Louis, Missouri, www.eas.slu.edu/People/RBHerrmann/GroundMotion (last accessed July 2015).

Sato, H. (1977). Energy propagation including scattering effects single isotropic scattering approximation, *J. Phys. Earth* **25,** 27–41.

Sato, H. (1984). Attenuation and envelope formation of three-component seismograms of small local earthquakes in randomly inhomogeneous lithosphere, *J. Geophys. Res.* **89,** 1221–1241.

Sato, H., and M. C. Fehler (1998). *Seismic Wave Propagation and Scattering in the Heterogeneous Earth*, American Institute of Physics Press, New York, New York.

Scherbaum, F., and C. Kisslinger (1985). Coda *Q* in the Adak seismic zone, *Bull. Seismol. Soc. Am.* **75,** 615–620.

Sertçelik, F. (2012). Estimation of coda wave attenuation in the east Anatolia fault zone, Turkey, *Pure Appl. Geophys.* **169,** 1189–1204.

Shengelia, I., Z. Javakhishvili, and N. Jorjiashvili (2011). Coda wave attenuation for three regions of Georgia (Sakartvelo) using local earthquakes, *Bull. Seismol. Soc. Am.* **101,** 2220–2230.

Singh, S., and B. Herrmann (1983). Regionalization of crustal coda *Q* in the continental United States, *J. Geophys. Res.* **88,** 527–538.

Talwani, P. (2014). *Intraplate Earthquakes*, University Press, Cambridge, United Kingdom.

Tavakoli, B., S. Pezeshk, and R. Cox (2010). Seismicity of the New Madrid seismic zone derived from a deep-seated strike-slip fault, *Bull. Seismol. Soc. Am.* **100,** 1646–1658.

Tripathi, J. N., P. Singh, and M. Sharma (2014). Attenuation of high-frequency *P*- and *S*-waves in Garhwal Himalaya, India, *Tectonophysics* **636,** 216–227.

Wennerberg, L. (1993). Multiple scattering interpretations of coda *Q* measurements, *Bull. Seismol. Soc. Am.* **83,** 279–290.

Wessel, P., and W. H. F. Smith (1998). New improved version of the Generic Mapping Tools released, *Eos Trans. AGU* **79,** 579.

Woodgold, C. R. D. (1994). Coda *Q* in the Charlevoix, Quebec, region: Lapse-time dependence and spatial and temporal comparisons, *Bull. Seismol. Soc. Am.* **84,** 1123–1131.

Wu, H., and J. M. Lees (1996). Attenuation structure of the Coso Geothermal area, California, from pulse width data of *P*-wave, *Bull. Seismol. Soc. Am.* **86,** 1574–1590.

Xie, J., and O. W. Nuttli (1988). Interpretation of high-frequency coda at large distances: Stochastic modeling and method of inversion, *Geophys. J. Int.* **95,** 579–595.

Yoshimoto, K., H. Sato, Y. Iio, H. Ito, T. Ohminato, and M. Ohtake (1998). Frequency-dependent attenuation of high-frequency *P* and *S* Waves in the upper crust in western Nagano, Japan, *Pure Appl. Geophys.* **153,** 489–502.

Yoshimoto, K., H. Sato, and M. Ohtake (1993). Frequency-dependent attenuation of *P* and *S* waves in the Kanto area, Japan, based on the coda-normalization method, *Geophys. J. Int.* **114,** 165–174.

Zandieh, A., and S. Pezeshk (2010). Investigation of geometrical spreading and quality factor functions in the New Madrid seismic zone, *Bull. Seismol. Soc. Am.* **100,** 2185–2195.

Zandieh, A., and S. Pezeshk (2011). A study of horizontal-to-vertical component spectral ratio in the New Madrid seismic zone, *Bull. Seismol. Soc. Am.* **101,** 287–296.

Zeng, Y. (1991). Compact solutions for multiple scattered wave energy in time domain, *Bull. Seismol. Soc. Am.* **81,** 1022–1029.

Zeng, Z., and J. G. Anderson (1996). A composite source model of the 1994 Northridge earthquake using genetic algorithms, *Bull. Seismol. Soc. Am.* **86,** 71–83.

Zhang, Q., E. Sandvol, and M. Liu (2009). Lithospheric velocity structure of the New Madrid seismic zone: A joint teleseismic and local *P* tomographic study, *Geophys. Res. Lett.* **36,** L11305, doi: 10.1029/2009GL037687.

Zollo, A., and S. de Lorenzo (2001). Source parameters and three-dimensional attenuation structure from the inversion of microearthquake pulse width data: Method and synthetic tests, *J. Geophys. Res.* **106,** 16,287–16,306.

Department of Civil Engineering
The University of Memphis
3815 Central Avenue
Memphis, Tennessee 38152
fsdghati@memphis.edu
spezeshk@memphis.edu

Manuscript received 1 December 2015;
Published Online 7 June 2016